JACS
JOURNAL OF THE AMERICAN CHEMICAL SOCIETY

Article

pubs.acs.org/JACS

Psoromic Acid is a Selective and Covalent Rab-Prenylation Inhibitor Targeting Autoinhibited RabGGTase

Céline Deraeve,[†,¶,⊥] Zhong Guo,[‡,#,⊥] Robin S. Bon,[†,◆] Wulf Blankenfeldt,[‡,○] Raffaella DiLucrezia,[∥] Alexander Wolf,[∥] Sascha Menninger,[∥] E. Anouk Stigter,[†] Stefan Wetzel,[†] Axel Choidas,[∥] Kirill Alexandrov,[‡,#] Herbert Waldmann,[†,§] Roger S. Goody,[‡] and Yao-Wen Wu*[,‡]

[†]Department of Chemical Biology and [‡]Department of Physical Biochemistry, Max Planck Institute of Molecular Physiology, Otto-Hahn-Strasse 11, 44227 Dortmund, Germany

[§]Technische Universität Dortmund, Fachbereich Chemie, 44227 Dortmund, Germany

[∥]Lead Discovery Center GmbH, Otto-Hahn-Strasse 15, 44227 Dortmund, Germany

Supporting Information

ABSTRACT: Post-translational attachment of geranylgeranyl isoprenoids to Rab GTPases, the key organizers of intracellular vesicular transport, is essential for their function. Rab geranylgeranyl transferase (RabGGTase) is responsible for prenylation of Rab proteins. Recently, RabGGTase inhibitors have been proposed to be potential therapeutics for treatment of cancer and osteoporosis. However, the development of RabGGTase selective inhibitors is complicated by its structural and functional similarity to other protein prenyltransferases. Herein we report identification of the natural product psoromic acid (PA) that potently and selectively inhibits RabGGTase with an IC_{50} of 1.3 μM. Structure−activity relationship analysis suggested a minimal structure involving the depsidone core with a 3-hydroxyl and 4-aldehyde motif for binding to RabGGTase. Analysis of the crystal structure of the RabGGTase:PA complex revealed that PA forms largely hydrophobic interactions with the isoprenoid binding site of RabGGTase and that it attaches covalently to the N-terminus of the α subunit. We found that in contrast to other protein prenyltransferases, RabGGTase is autoinhibited through N-terminal $_{\alpha}$His2 coordination with the catalytic zinc ion. Mutation of $_{\alpha}$His dramatically enhances the reaction rate, indicating that the activity of RabGGTase is likely regulated in vivo. The covalent binding of PA to the N-terminus of the RabGGTase α subunit seems to potentiate its interaction with the active site and explains the selectivity of PA for RabGGTase. Therefore, psoromic acid provides a new starting point for the development of selective RabGGTase inhibitors.

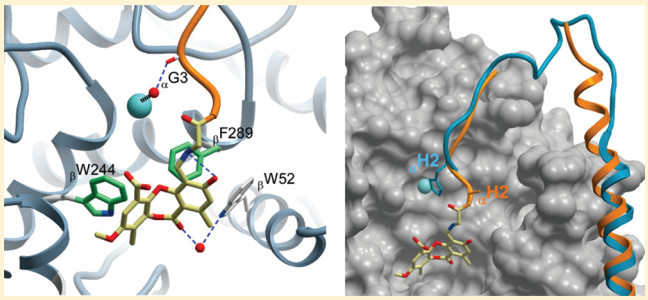

INTRODUCTION

Post-translational modification of proteins with isoprenoids, known as prenylation, is a vital process affecting hundreds of proteins controlling signal transduction and cargo transport in eukaryotic cells. This process involves the covalent attachment of either a 15-carbon farnesyl or a 20-carbon geranylgeranyl group to conserved C-terminal cysteine residues. The lipid modification enables prenylated proteins to reversibly associate with intracellular membranes.[1] The major substrates of protein prenylation include the signal transducing Ras superfamily of small GTPases. Rab GTPases, with over 60 members in humans, constitute the largest subgroup of the Ras superfamily. Rab GTPases play key roles in the regulation of intracellular membrane trafficking through association with specific membranes and the recruitment of an array of specific effector proteins responsible for transport, tethering/docking, and fusion of vesicles.[2]

Prenylation of Rab proteins is mediated by Rab geranylgeranyltransferase (RabGGTase). RabGGTase covalently attaches two (in a few cases one) geranylgeranyl moieties to two cysteine residues at the C-terminus of Rab proteins. Unlike the other protein prenyltransferases, farnesyltransferase (FTase) and geranylgeranyltransferase I (GGTase I), which recognize a C-terminal CAAX box, RabGGTase requires an accessory Rab escort protein (REP) to recruit Rab proteins with diversified C-terminal sequences.

Inhibition of RabGGTase has been proposed to be exploitable for the treatment of several human diseases. A weak but specific RabGGTase inhibiting phosphonocarboxylate (PC) has been identified and was considered as a lead drug candidate for the treatment of thrombotic disorders and osteoporosis and for antitumor therapy.[3,4] More recent studies have shown that inhibition of RabGGTase induces p53-independent apoptosis in tumor cells and validated this enzyme as a promising target for cancer chemotherapy.[5] It was

Received: December 7, 2011
Published: April 5, 2012

   dx.doi.org/10.1021/ja211305j | J. Am. Chem. Soc. 2012, 134, 7384−7391

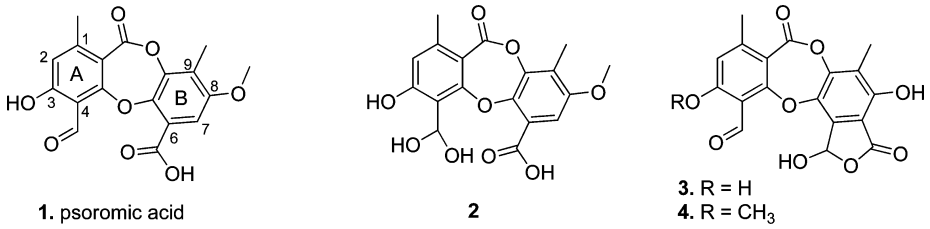

Figure 1. Structures of PA family members identified as RabGGTase inhibitors.

Table 1. IC_{50} Values and Selectivity for the Inhibition of RabGGTase by PA and Analogues*

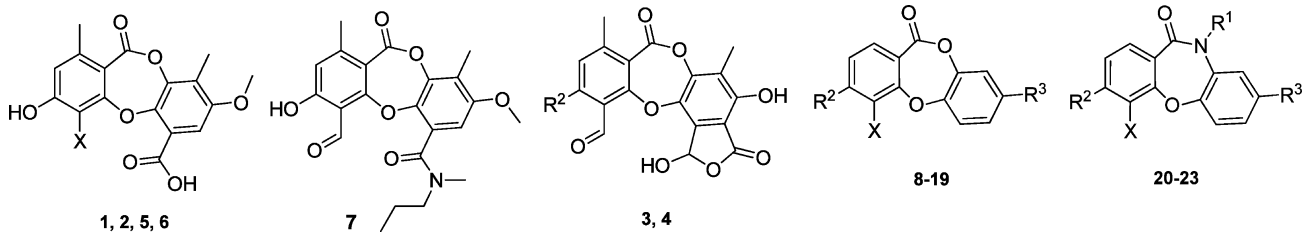

Entry	Cmpd.	R^1	R^2	R^3	X	IC_{50} [μM] RabGGTase[a]	RabGGTase[b]	FTase[b]	GGTase-I[b]
1	**1**	-	-	-	-CHO	1.4 ± 0.1	1.3 ± 0.1	> 100	78 ± 3.4
2	**2**	-	-	-	$-CH(OH)_2$	16.7 ± 2.9	-	-	-
3	**3**	-	-OH	-	-	3.1 ± 0.2	-	-	-
4	**4**	-	-OMe	-	-	5.5 ± 0.4	-	-	-
5	**5**	-	-	-	-COOH	> 100	-	-	-
6	**6a**	-	-	-	-C=N-OH	> 100	-	-	-
7	**6b**	-	-	-	-C=N-OMe	> 100	-	-	-
8	**6c**	-	-	-	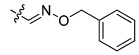	19.7 ± 2.2	-	-	-
9	**6d**	-	-	-	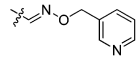	> 100	-	-	-
10	**6e**	-	-	-	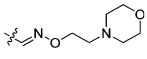	> 100	-	-	-
11	**7**	-	-	-	-	31.9 ± 24.5	-	-	-
12	**8**	-	-H	-H	$-CH_3$	> 100	-	-	-
13	**9**	-	-H	-H	$-CO_2Me$	> 100	-	-	-
14	**10**	-	-H	-H	$-CO_2H$	> 100	-	-	-
15	**11**	-	-H	-OMe	$-CH_3$	> 100	-	-	-
16	**12**	-	-H	OMe	-CHO	> 100	-	-	-
17	**13**	-	-OiPr	-H	-CHO	~ 50	-	-	-
18	**14**	-	-OH	-H	-CHO	6.1 ± 0.8	7.9 ± 2.7	> 100	68 ± 14
19	**15**	-	-OiPr	-OMe	$-CH_3$	> 100	-	-	-
20	**16**	-	-OiPr	-OMe	$-CH_2Br$	partial inhibition [c)]	-	-	-
21	**17**	-	-OiPr	-OMe	$-CH_2OH$	~ 80	-	-	-
22	**18**	-	-OiPr	-OMe	-CHO	29.3 ± 0.3	-	-	-
23	**19**	-	-OH	-OMe	-CHO	4.2 ± 0.3	6.3 ± 2.5	> 100	32 ± 4.3
24	**20**	-H	-OMe	-H	-CHO	31.4 ± 14.9	-	-	-
25	**21**	-H	-OH	-H	-CHO	15.6 ± 13.0	-	-	-
26	**22**	-H	-OH	-H	$-CH_2OH$	> 100	-	-	-
27	**23**	-Me	-OH	-H	-CHO	38.1 ± 30.1	-	-	-

*IC_{50} values were determined by at least three independent measurements by means of (a) a fluorometric assay (plate assay) for RabGGTase and (b) a SDS-PAGE assay (gel assay) for the three protein prenyltransferases. (c) Dose-dependent inhibition was observed in this case but was found to be saturated at 50% of inhibition.

dx.doi.org/10.1021/ja211305j | J. Am. Chem. Soc. 2012, 134, 7384−7391

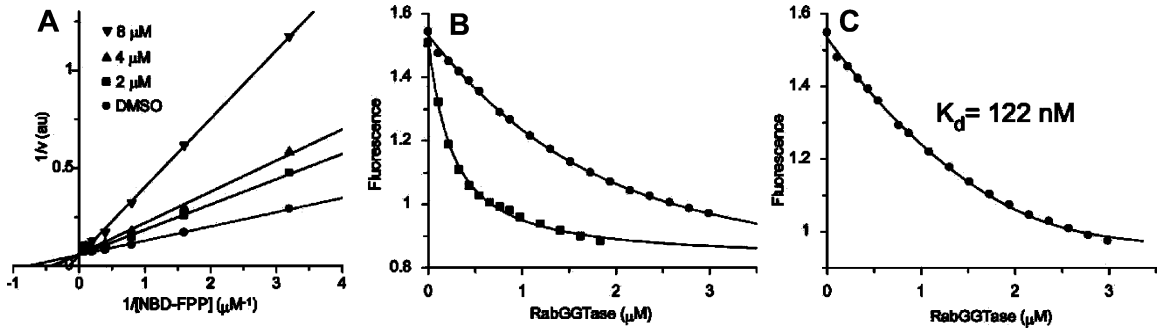

Figure 2. Inhibition of RabGGTase by PA **1**. (A) Lineweaver–Burk plot with NBD-FPP as varied substrate at indicated PA concentrations. The velocity, v, is expressed in arbitrary units. (B) Titration of 400 nM NBD-FPP in the absence (■) and the presence of 2 μM PA (●) with RabGGTase. The data were fitted with a quadratic equation to give a K_d of 73 ± 22 nM for the binding of NBD-FPP to RabGGTase and an apparent K_d^{app} value of 1.9 ± 0.1 μM for the binding in the presence of PA. (C) The same data as in (B) in the presence of PA were fitted by numerical simulation to a competitive titration model to give a genuine K_d value of 122 ± 6 nM for the RabGGTase:PA interaction.

Scheme 1. Synthesis of PA analogues via modification of the natural product (A) and by de novo synthesis in the lactone series (B) or in the lactam series (C)*

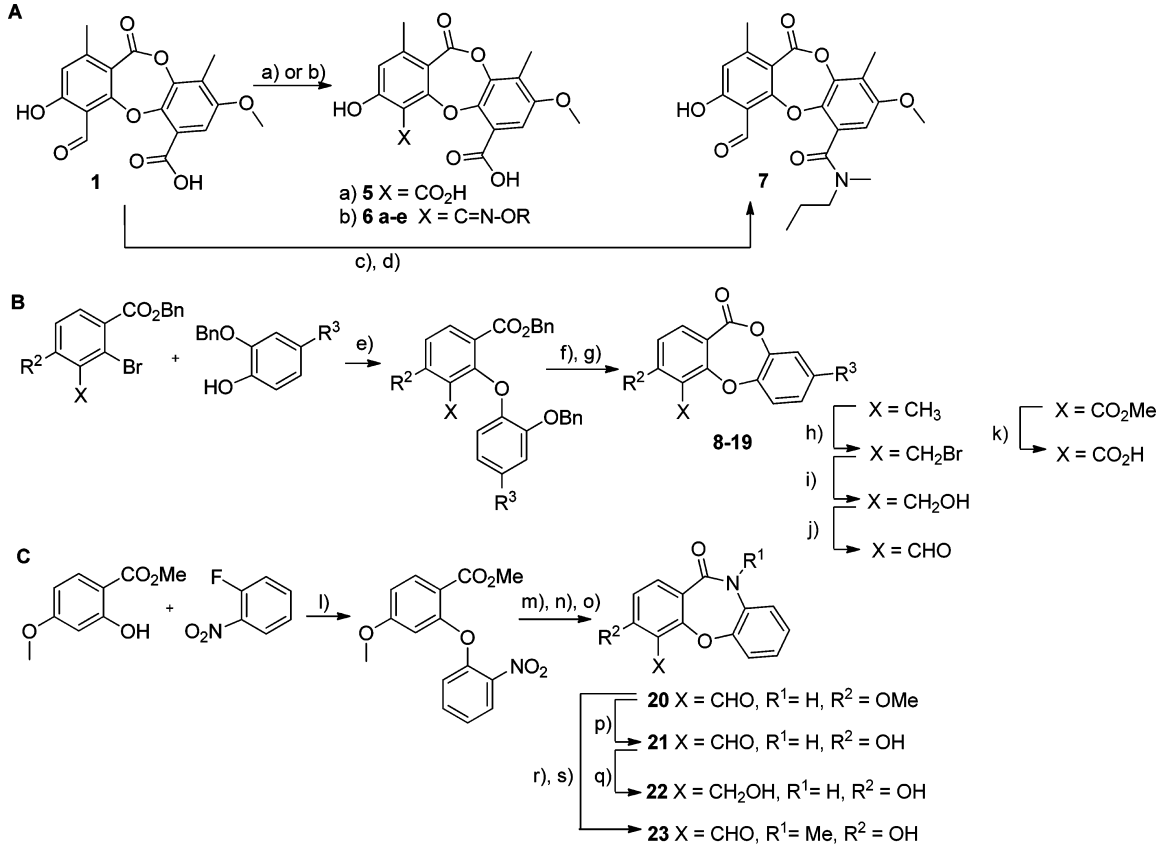

*(a) $NaClO_2$, NaH_2PO_4, DMSO/H_2O, rt, 72 h, 53%; (b) $RONH_2$·HCl, pyridine, rt, 4–24 h, 47% to quant.; (c) $(COCl)_2$, CH_2Cl_2, rt, 16 h; (d) *N*-methylpropan-1-amine, CH_2Cl_2, rt, 1 h, 29% over 2 steps; (e) CuO, K_2CO_3, pyridine, 130 °C, 48 h, 54–77%; (f) H_2, Pd/C, EtOAc, rt, 6 h; (g) $SOCl_2$, Et_2O, rt, 24 h, 64–96% over 2 steps; (h) NBS, AIBN, CCl_4, 70 °C, 8 h, 59–90%; (i) dioxane/H_2O, 100 °C, 6 h, 51% to quant.; (j) PCC, CH_2Cl_2, rt, 7 h, 64–92%; (k) LiCl, DMF, 130 °C, 8 h, 72%; (l) K_2CO_3, DMF, 60 °C, 16 h, 65%; (m) $Pd(OH)_2$/C, $HCOONH_4$, EtOH 60 °C, 2 h, 79%; (n) H_2SO_4 conc., DMF, 150 °C, 16 h, 69%; (o) BuLi, TMEDA, THF, 65 °C, 2 h, then DMF, 65 °C, 2 h, 42%; (p) BBr_3, CH_2Cl_2, rt, 1 h, 22%; (q) $NaBH_4$, EtOH, rt, 16 h, 37%; (r) NaH, MeI, DMF, rt, 16 h, 71%;(s) BBr_3, CH_2Cl_2, rt, 1 h, 23%. NBS, *N*-bromosuccinimide; AIBN, azobisisobutyronitrile; PCC, pyridinium chlorochromate; DMF, dimethylformamide; TMEDA, tetramethylenediamine; and THF, tetrahydrofuran.

proposed that the inhibition of RabGGTase may be at least partially responsible for the proapoptotic action of several FTase inhibitors that are currently in late-stage clinical trials.[5] In addition, overexpression of RabGGTase and a few Rab proteins has been reported in several cancer types.[6] Furthermore, overexpression of Rab25 in breast and ovarian cancer cells was reported to increase the aggressiveness of these cancers.[6,7] Potent and selective RabGGTase inhibitors could provide invaluable tools for the study of Rab prenylation and its role in skeletal disorders and cancer and offer new starting points for the development of drug candidates. However, the availability of such compounds is rather limited.[8−12] Herein we

dx.doi.org/10.1021/ja211305j | J. Am. Chem. Soc. 2012, 134, 7384–7391

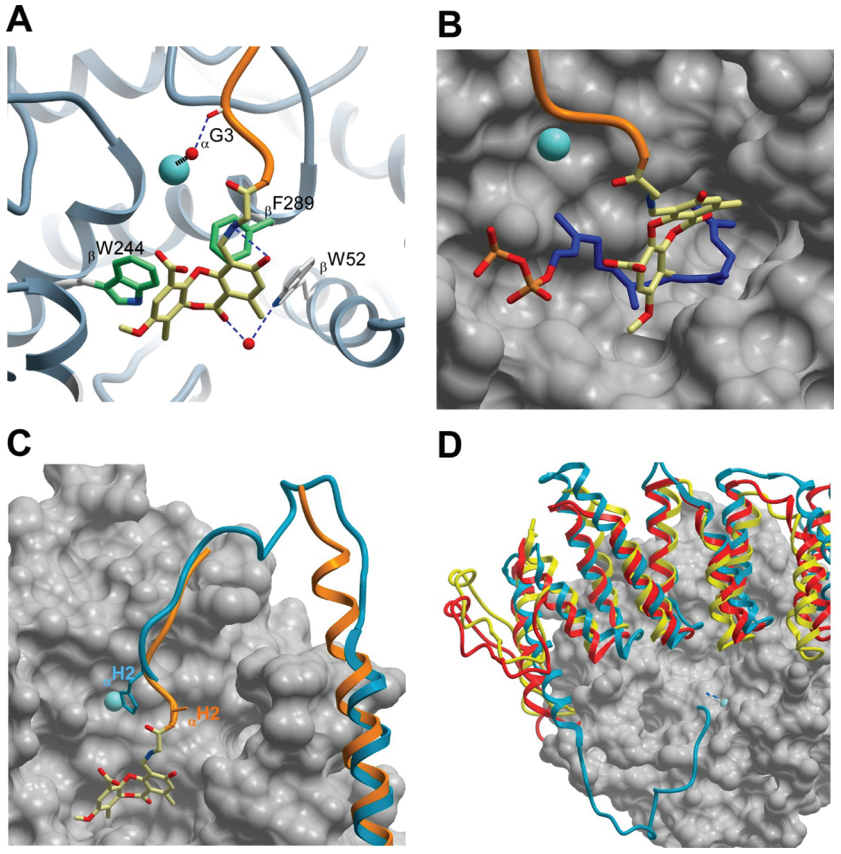

Figure 3. Structural analysis of RabGGTase complexed with PA and apo-RabGGTase. (A) Binding of PA to the active site of RabGGTase. The β subunit of RabGGTase is displayed as gray ribbons. The N-terminus of RabGGTase covalently linked to PA is displayed as an orange worm. PA and the interacting side chains of the β subunit are displayed as sticks colored by atom type. The side chains of $_{\beta}$F289 and $_{\beta}$W244 involved in hydrophobic interaction with PA are colored in green. Blue dashed lines indicate hydrogen bonds. The water molecules involved in hydrogen bonding are displayed as red spheres. The zinc ion is shown as a cyan sphere. (B) Superimposition of the structures of RabGGTase in complex with PA and GGPP (PDB code: 3DST). The β subunit of RabGGTase is displayed in gray surface representation. In both figures, the α subunit and the side chain of $_{\alpha}$Met1 have been omitted for clarity. PA is displayed as sticks colored by atom type. The geranylgernyl chain of GGPP is shown in blue, and the pyrophosphate head is shown in red. (C) Superimposition of the structures of apo-RabGGTase (PDB code: 1DCE) and RabGGTase complexed with PA. The β subunit of RabGGTase is displayed in gray surface representation. The α subunits of apo-RabGGTase and RabGGTase complexed with PA are displayed as blue and orange ribbons. The side chain of apo-RabGGTase $_{\alpha}$H2 that coordinates the zinc ion is shown as blue sticks. Because the electron density of $_{\alpha}$H2 side chain in the RabGGTase:PA complex was not visible, it is represented as an alanine. (D) Superimposition of the structures of apo-RabGGTase, FTase and GGTase-I (PDB code: 1DCE, 1FT1, and 1N4P). The β subunit of RabGGTase is displayed in gray surface representation. The α subunits of RabGGTase, FTase, and GGTase-I are displayed as blue, golden, and red ribbons, respectively. The side chain of RabGGTase $_{\alpha}$H2 that coordinates the zinc ion is shown as sticks colored by atom type.

report the identification of the natural product psoromic acid (PA), and analogues thereof, as a new class of potent and selective RabGGTase inhibitors. The crystal structure of the RabGGTase:PA complex provided insights into the binding mode and explained the selectivity of the compound.

RESULTS AND DISCUSSION

We screened a library of 13 030 compounds including 3967 natural products, 1418 small molecules, and 7645 semisynthetic compounds using a fluorometric Rab prenylation assay that monitors the change of fluorescence observed upon transfer of NBD-farnesyl pyrophosphate (NBD-FPP), a fluorescent analogue of the lipid substrate geranylgeranyl pyrophosphate (GGPP).[13,14] A prescreen at a concentration of 100 μM was used to identify compounds that inhibit RabGGTase, and the compounds that displayed more than 70% inhibition were selected for concentration-dependent measurements. PA **1** (Figure 1) was found to be a relatively potent inhibitor of RabGGTase, with an IC_{50} value of 1.4 $\pm$ 0.1 μM. Additional compounds embodying the PA core structure displayed appreciable inhibitory activity, suggesting that the PA core defines the scaffold of a new RabGGTase inhibitor class (Figure 1). These compounds belong to the depsidones, a family of lichen secondary metabolites. Depsidones exhibit a range of biological activities including antioxidant, inhibition of 5-lipoxygenase, and inhibition of HIV-1 integrase.[15−17] The apoptotic activity of PA was documented.[18]

We further evaluated the inhibitory activity of PA toward the other protein prenyltransferases, FTase and GGTase-I, using a SDS-PAGE in vitro prenylation assay. Interestingly, PA showed selective inhibition of RabGGTase over FTase and GGTase-I by a factor of more than 100 and 60, respectively (Table1).

The inhibition mode of PA and its affinity for RabGGTase were then examined using the fluorometric assay using NBD-FPP. PA was found to be a competitive inhibitor with respect to the lipid substrate (Figure 2A). The fluorescence change upon binding of NBD-FPP to RabGGTase was used to perform titrations to determine binding affinities. An inhibition of NBD-

dx.doi.org/10.1021/ja211305j | J. Am. Chem. Soc. 2012, 134, 7384−7391

FPP binding to RabGGTase was observed in the presence of PA. The affinity of RabGGTase:NBD-FPP was weakened by a factor of ca. 30 in the presence of 2 μM PA (Figure 2B). This is in line with competitive binding of PA versus NBD-FPP. Fitting of the data by numerical simulation with a competitive model led to a genuine K_d of 122 ± 6 nM for binding of PA to RabGGTase (Figure 2C). These results suggest that PA is a potent and selective inhibitor of RabGGTase. In particular, the chemotype represented by the PA core provides a promising starting point for the development of RabGGTase inhibitors.

Preliminary structure−activity relationship (SAR) studies indicate that the aldehyde function is required for the activity of the natural product (Figure 1). The carboxylic acid group is dispensable, since compounds **3** and **4** showed good inhibitory activity toward RabGGTase.

To refine the SAR profile, a series of PA analogues was synthesized either by modification of the natural product or by de novo synthesis. The reactivity of the aldehyde function of PA was used to obtain access to the 4,6-dicarboxylic acid **5** or to obtain a series of oximes **6**. The carboxylic group at the 6-position was converted to the amide **7** (Scheme 1A). In addition, PA analogues were synthesized via a route derived from a previous total synthesis of PA (Scheme 1B).[19,20] The key formation of the diaryl ether bond was achieved by means of a modified Ullmann procedure using copper(II) oxide as catalyst. Substantial variations of the reaction conditions (copper or palladium catalysts, base, coligands and solvent) did not lead to general improvement of yields. Removal of the benzyl protecting groups by palladium/carbon-catalyzed hydrogenation and subsequent conversion of the acid into the acid chloride led to the formation of seven-membered ring lactones. The aldehyde function at the 4-position was then introduced by oxidation of the methyl group through monobromination, hydrolysis, and oxidation of the resulting primary alcohol, followed by deprotection reactions when required.

Compounds **5** and **6** displayed significantly lower inhibitory activity (Table 1), suggesting that the aldehyde function at the 4-position plays a decisive role in generating the potency of PA-derived inhibitors. This prompted us to examine whether PA could form a Schiff base with the enzyme. Subsequent ESI-MS analysis indeed indicated that one PA molecule was attached to each subunit of RabGGTase as well as those of FTase and GGTase-I when these enzymes were incubated with PA (Supporting Information, Figure S1). The single modification of each subunit of the proteins by PA suggests that it may selectively form a Schiff base with the N-terminal amine or a lysine residue.

To gain more insight into the principles governing the binding of PA, we attempted to determine the crystal structure of PA-bound RabGGTase with IGG and LRR domains truncated. In our previous work, the engineered RabGGTase has dramatically improved crystallization properties and displayed identical enzymatic activity to the wild-type enzyme.[9,21] Since the imine bond is not stable under X-ray exposure, RabGGTase crystals were soaked with 1 mM PA and were subsequently treated with 80 mM $NaCNBH_3$ to reduce the imine to a stable amine. The structure was determined at 2.2 Å resolution. The crystal structure revealed that PA binds covalently to the N-terminal amine of the RabGGTase α subunit, and the interaction of PA with RabGGTase is largely hydrophobic, involving hydrophobic interaction of two phenyl rings with $_\beta$Trp244 and $_\beta$Phe289 and a weak hydrogen bond between the lactone carbonyl and $_\beta$Trp52 via a water molecule (Figure 3A). The N-terminal residues of the RabGGTase α subunit ($_\alpha$His2 to $_\alpha$Glu22) are flexible, and only the electron density of the main chain spanning $_\alpha$His2 to Val6 located near the active site could be traced (Figure 3C). The interaction of the N-terminal region of the α subunit with the β subunit in the RabGGTase:PA structure involves hydrogen bonding of the main-chain carbonyl of $_\alpha$Leu5 with the amide of $_\beta$Met285, the main-chain carbonyl of $_\alpha$Gly3 with the water molecule that coordinates the zinc ion, and the side chain of $_\alpha$Met1 with $_\beta$Tyr44 (Figure 3A).

In the apo-RabGGTase structure, the N-terminal region of the α subunit binds to the β subunit in an extended conformation with $_\alpha$His2 coordinating the catalytic zinc ion (Figure 3C,D).[22] Such an interaction was not observed in FTase and GGTase-I structures (Figure 3D).[23] Together with the fact that the aldehyde group is indispensable for the inhibitory activity of PA-derived compounds (Table 1), it is conceivable that the covalent binding of PA to the N-terminus of RabGGTase α subunit enhances the binding of PA to the active site. Because the observed interaction of the N-terminal region of the α subunit was significantly altered in the RabGGTase:PA structure compared with the apo-RabGGTase structure (Figure 3C), the PA binding to the active site plays a predominant role in the RabGGTase:PA interaction. Thus, it appears that PA binding with the active site governs the specificity of the interaction with RabGGTase. Superimposition of the RabGGTase:PA structure with RabGGTase in complex with the lipid substrate GGPP revealed that the phenyl ring B of PA occupies the binding site of the second isoprenyl unit of GGPP (Figure 3B). The structure is consistent with the competitive binding mode as determined above.

Comparing to other so far identified RabGGTase inhibitors, PA is the only one that displays such a binding mode, i.e., associates with the lipid binding site and covalently binds to the N-terminal amine of the α subunit. The tetrahydrobenzodiazepine (THB) and peptide inhibitors of RabGGTase coordinate the catalytic zinc ion, whereas PA does not. THB and peptide inhibitors achieve selectivity toward RabGGTase by targeting the TAG tunnel (tunnel adjacent to the GGPP binding site), which is unique in RabGGTase.[8,9,11] In contrast, PA does not associate with the TAG tunnel. PA is much more potent than the first selective RabGGTase inhibitor (IC_{50} = 560 μM), NE10790, a PC analogue of bisphosphonate risedronate (RIS).[3] Recently, a new series of PC analogue of RIS has been developed with IC_{50}s of 1−50 μM toward RabGGTase and no obvious inhibition of GGTase-I at milimolar concentration.[10] Allenoate-derived compounds showed low micromolar inhibition of both RabGGTase and GGTase-I, but no apparent inhibition of FTase at 100 μM.[12] The submicromolar THB inhibitors, low micromolar peptide inhibitors, and PA display similar selectivity for RabGGTase over FTase and GGTase-I,[8,11] suggesting it is possible to develop potent and selective RabGGTase inhibitors combining rational design and high-throughput screening.

Among other compounds, only **19** and **14** were identified as potent inhibitors of RabGGTase with IC_{50} values of 4.2 ± 0.3 and 6.1 ± 0.8 μM, respectively. These findings demonstrate that the removal of the carboxylic acid and both methyl groups from PA led only to a slight decrease of activity (compound **19**, Table 1 entry 23), suggesting that these functions are not essential for RabGGTase inhibition. Similarly, the methoxy group at the 8-position can be omitted without pronounced influence on the activity (compound **14**, Table 1 entry 18).

dx.doi.org/10.1021/ja211305j | J. Am. Chem. Soc. 2012, 134, 7384−7391

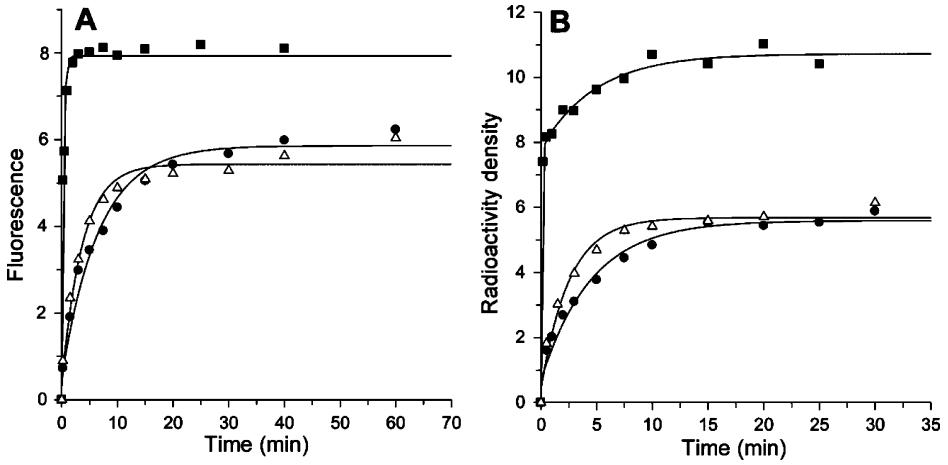

Figure 4. Single-turnover prenylation by RabGGTase variants. (A) SDS-PAGE assay using NBD-FPP. The solid lines show single exponential fits, giving k_{obs} of 0.15, 0.27, and 3.4 min^{-1} for wild-type RabGGTase (●), ΔM1 (△), and H2A (■), respectively. (B) Prenylation assay using H^3-GGPP. The solid lines show single exponential fits, giving k_{obs} of 0.22 and 0.4 for wild type RabGGTase (●) and ΔM1 (△), respectively, and a double exponential fit for H2A mutant (■), giving the k_{obs} of 13 and 0.2 min^{-1} for the fast and slow phases, respectively.

These results are in line with the structural analysis, since these groups were not involved in apparent interactions and the contact of PA with RabGGTase arose mainly from hydrophobic interaction of two phenyl rings. Comparison of the results for **18** and its precursors **15**−**17** (Table 1, entries 19−22) again stresses the crucial role of the aldehyde function for RabGGTase inhibition by this class of compounds. The hydroxyl group at the 3-position is required, since its omission led to loss of the inhibitory activity (compound **12**, Table entry 16). Substitution of the 3-hydroxyl with a methoxyl group led to a moderate reduction of the inhibitory activity (compare **4** with **3** and **20** with **21**), whereas substitution with a larger isopropoxyl group resulted in substantial reduction of the inhibitory activity (compare **13** with **14** and **18** with **19**). Structural analysis indicated that the 3-hydroxyl may be involved in hydrogen bonding with the Schiff base, which could stabilize the Schiff base (Figure 3A). These results suggest that **14**, which incorporates the depsidone core structure and a 3-hydroxyl and 4-aldehyde motif, represents a minimal structure in the PA series for RabGGTase inhibition. Interestingly, simplified PA analogues **14** and **19** retained the selectivity for RabGGTase with respect to FTase and GGTase-I (Table 1, entries 18 and 23). Replacement of the lactone of the depsidone core structure by a more stable lactam function was also investigated. A series of lactam analogues was prepared on the basis of the minimal scaffold represented by compound **14** (Scheme 1C) and was evaluated for RabGGTase inhibition (Table 1). Such a replacement did not affect the inhibitory potency of the compounds, (compare **14** with its lactam analogue **21**, Table 1 entries 18 and 25). As expected, the aldehyde function is crucial for the binding (**22**, Table 1 entry 26). N-methylation of the lactam led to a three-fold decrease in the inhibitory activity (**23**, Table 1 entry 27). Coherently the crystal structure suggested that such a modification leads to a steric clash with $_{\beta}$Trp244.

RabGGTase inhibition in HeLa cells was determined by reprenylation assay using biotin-GPP, where unprenylated Rab proteins in cells were detected.[11] Neither cytotoxicity nor inhibition of RabGGTase was observed when the cells were treated with PA in various concentrations (1−300 μM). In contrast, treatment with compactin, which inhibits the biosynthesis of isoprenoids, led to accumulation of unprenylated Rab proteins (Figure S4, Supporting Information). The low efficiency of PA to affect cellular prenylation might be partially due to its moderate membrane permeability. As determined by the parallel artificial membrane permeation assay (PAMPA) using an artificial lipid bilayer, PA displayed dramatically lower membrane permeability than the control compound, BMS3, which has been proved to be active in cells (Figure S5, Supporting Information).[8] The THB and peptide inhibitors were shown to inhibit RabGGTase in cells with IC_{50}s of 10−400 nM and 10−50 μM, respectively.[8,11] The first selective RabGGTase inhibitor, NE10790, inhibited RabGGTase activity in cells with an IC_{50} of ∼600 μM.[3] The most potent PC analogue of bisphosphonate risedronate displayed the lowest effective dose of 3 μM for inhibition of Rab11 prenylation in cells.[10] Slight inhibition of Rab5b prenylation in cells was observed with the treatment of 20 μM one of allenoate-derived compounds.[12] Further alterations of PA structure to improve its cellular activity will be carried out in future studies.

The association of the N-terminal region of the α subunit with the active site suggests an autoinhibitory mechanism in RabGGTase.[22] Observation of the coordination of $_{\alpha}$His2 with the catalytic zinc ion in the apo-RabGGTase structure prompted us to ask what the consequence of such an interaction is. $_{\alpha}$His2 is conserved in RabGGTase in mammals and yeast (Supporting Information, Figure S3). However, this histidine residue is not present in FTase and GGTase-I. To this end, RabGGTases with N-terminal mutations were subjected to the in vitro prenylation assay. Remarkably, the $_{\alpha}$H2A mutant displayed an observed rate of 3.4 min^{-1} in a single turnover reaction using NBD-FPP, which was more than 20-fold faster than the wild-type enzyme (k_{obs} = 0.15 min^{-1}). In contrast, truncation of $_{\alpha}$Met1 (ΔM1) only led to a slight increase of the reaction rate (k_{obs} = 0.27 min^{-1}) (Figure 4A). Similar results were obtained in the prenylation assay using tritium-labeled GGPP (Figure 4B). These results suggested that RabGGTase is autoinhibited through the coordination of $_{\alpha}$His2 with the catalytic zinc ion. The functional role of RabGGTase autoinhibition remains elusive. However, it appears that this feature is exploited by PA to achieve selectivity for RabGGTase.

The question of the function or purpose of RabGGTase autoinhibition is an intriguing one. RabGGTase is a much

dx.doi.org/10.1021/ja211305j | J. Am. Chem. Soc. 2012, 134, 7384−7391

slower enzyme than FTase or GGTase-I, but the results described here demonstrate that a single amino acid substitution dramatically increases the reaction rate. It therefore appears likely that the low intrinsic activity is of physiological significance. One possibility is that maximal activity is only developed on interaction with an as yet unidentified activation factor in vivo.

CONCLUSIONS

In conclusion, we have identified the natural product PA as a new potent and selective inhibitor of RabGGTase. SAR analysis with analogues of PA led to identification of a minimal structure, involving the depsidone core structure and a 3-hydroxyl and 4-aldehyde motif, for selective inhibition of RabGGTase. The crystal structure of RabGGTase in complex with PA revealed that the interaction involves hydrophobic interactions of PA with the isoprenoid binding site and hydrogen bonding between the N-terminal region of the α and β subunits. We conclude that the covalent binding of PA to the N-terminus of the α subunit enhances the binding of PA to the active site. However, neither cytotoxicity nor inhibition of RabGGTase was observed in cells treated with PA up to 300 μM. Biochemical experiments confirmed that the autoinhibition of RabGGTase is resulted from coordination of N-terminal $_{\alpha}$His2 with the catalytic zinc ion. Taken together, the SAR profile and mapping of the interactions between PA and the enzyme in the crystal structure of the complex provide essential guidance for the design of new RabGGTase inhibitors.

METHODS

Synthesis and Characterization of the Compounds. For full details, refer to the Supporting Information.

Protein Expression and Purification. Rat REP-1 was cloned into pFastBacHTb (Invitrogen) with N-terminal His tag and was expressed in SF21 cells. The α and β subunits of rat FTase, GGTase-I, and RabGGTase variants were cloned into pGATEV and pET vectors, respectively. Both subunits were coexpressed in *Escherichia coli*. Human K-Ras, human RhoA, and canine Rab7 were cloned into pGATEV vector as N-terminal His-GST fusions and were expressed in *E. coli*. All proteins were purified by nickel-nitrilotriacetic acid affinity chromatography. After cleavage by tobacco etch virus (TEV) protease, the proteins were further purified by size exclusion chromatography.

Fluorometric Assay (Plate Assay). All solution-based enzyme assays were performed by means of an automated system consisting of a Zymark SciClone ALH 500 in conjunction with a Tecan 18 Genius Pro reader, using black 384-well plates. All inhibition measurements were performed in triplicate and measured under the following conditions: 37 °C, buffer: 50 mM HEPES, pH 7.2, 50 mM NaCl, 2 mM MgCl2, 2 mM DTE, 20 μM GDP, and 0.01% Triton X-100. Final concentrations: 3 μM Rab, 3 μM REP, 400 nM RabGGTase, 9 μM NBD-FPP **60**, and 100 μM test compound (from a 10 mM solution in DMSO). For the 100% activity control, instead of the test compound, 1% of DMSO was added. A 0% activity control was measured for every screened compound to enable correction of potential fluorophore bleaching and nonspecific effects of the test compound on the fluorescent signal. The 0% activity control wells contained 400 nM RabGGTase, 9 μM NBD-FPP, and 100 μM test compound in 10 μL of assay buffer. On every plate, a reference inhibitor was used for interplate control. After mixing of the fluorescent substrate, the enzyme, and the compound solutions (or DMSO), the reaction mixtures were incubated for 5 min at 37 °C. Then, the protein substrates (Rab7 and REP1) were added and fluorescence intensity was recorded for 30 min at intervals of 14 s (λ_{ex} = 479 nm, λ_{em} = 520 nm). Data were evaluated using Microsoft Excel. The fluorescence intensity at individual time points was normalized with respect to the 0% activity control, and reaction rates were determined from the linear parts of the progress curve. Compounds causing a residual RabGGTase activity of less than 30% were selected for IC_{50} determination. Concentration-dependent inhibition of RabGGTase was measured using different concentrations of inhibitors resulting from a two-fold dilution series. Reaction progress at every concentration of inhibitor was measured in triplicate, and 0% activity controls were measured for every inhibitor at every concentration. IC_{50} values were calculated using a four-parameter equation.[14]

SDS-PAGE Assay (Gel Assay) To Investigate Selectivity of Inhibitors. In the prenylation buffer (50 mM HEPES, pH 7.2, 50 mM NaCl, 2 mM $MgCl_2$, 2 mM DTE, and 0.01% Triton X-100), a 10 μL mixture of FTase with NBD-GPP, GGTase-I with NBD-FPP, and RabGGTase with NBD-FPP in the presence and the absence of various concentrations of inhibitor was incubated for 5 min at 37 °C, the same volume of protein substrate GST-KRas, GST-RhoA, and Rab7 with REP-1 was added to initiate the reaction. For the FTase assay, 3 μM GST-KiRas, 2 μM NBD-GPP, and 20 nM FTase, for the GGTase-I assay 6 μM GST-RhoA, 6 μM NBD-FPP, and 1 μM GGTase-I, for the RabGGTase assay 3 μM Rab, 3 μM REP-1, 2 μM NBD-FPP, and 40 nM RabGGTase were used, respectively. In the negative controls, the enzymes were omitted. Reactions were run for the same period of time (10 min) and quenched by adding cold 2 × SDS sample buffer. The reaction mixtures were resolved by 15% SDS-PAGE, and the gel was scanned using a Fluorescent Image Reader FLA-5000 (Fujifilm) (excitation laser at 473 nm and emission cutoff filter at 510 nm). The fluorescent bands corresponding to the formation of the prenylated product were quantified using the AIDA densitometry software. The data were processed in the same way as in the plate assay.

In vitro Prenylation Assay of RabGGTase Variants. A mixture of 10 μM Rab7 and RabGGTase variants with 100 μM NBD-FPP in prenylation buffer (50 mM HEPES, pH 7.2, 50 mM NaCl, 5 mM DTE, 2 mM $MgCl_2$, and 20 μM GDP) was added to 10 μM REP-1 to start the reaction. In the negative control, the REP-1 was omitted. At defined time intervals, 10 μL of reaction mixture were withdrawn, and the reactions were quenched by adding 10 μL 2 × SDS-loading buffer. After boiling at 95 °C for 5 min, the samples were resolved by 15% SDS-PAGE, and fluorescence intensities of the bands corresponding to the NBD-farnesylated Rab7 were measured and quantified as described above.

The prenylation assay using radioactive H^3-GGPP, which is the native lipid substrate, was performed with these RabGGTase variants. In the prenylation buffer, 2 μM of REP-1 was added to a mixture of 2 μM Rab7, RabGGTase,and H^3-GGPP and 8 μM unlabeled GGPP to start the reaction. At each time point, 20 μL of the reaction mixture was subjected to nitrocellulose paper. After 3× washing with 0.75% H_3PO_4, the intensity of radioactivity on the paper was measured under a Wallac MicroBeta TriLux 1450 LSC and Luminiscence Counter (PerkinElmer) and was quantified by a MicroBeta Windows Workstation (version V4.70.05).

Data Collection and Structural Determination of the RabGGTase:PA Complex. RabGGTaseΔLLRΔIG, in which the LRR and IG domain were deleted, was crystallized as described before.[9] The RabGGTase crystals were soaked in cryo-protecting buffer containing 1 mM PA for 1 h and were subsequently treated with 80 mM $NaCNBH_3$ overnight. Diffraction data were collected at 100 K at station X10SA of the Swiss Light Source (SLS, Villigen, Switzerland) or at a copper rotating X-ray anode with an osmic mirror (λ = 1.5419 Å, 50 kV, 100 mA, 0.1 mm collimator) (in-house). Structures were determined at 2.2 Å resolution using in-house X-ray sources. Full data collection and refinement statistics are summarized in Supporting Information Table S1. $|F_OF_C|$ difference electron density is shown in Supporting Information Figure S2. The coordinate has been deposited in the Protein Data Bank with accession number 4EHM.

■ ASSOCIATED CONTENT

Supporting Information

Full experimental detail, synthesis and characterization of compounds, ESI-MS measurements of covalent modifications, X-ray data collection, and refinement statistics, and $|F_O F_C|$ difference electron density map. This material is available free of charge via the Internet at http://pubs.acs.org.

■ AUTHOR INFORMATION

Corresponding Author

yaowen.wu@mpi-dortmund.mpg.de

Present Addresses

[#]Institute for Molecular Bioscience The University of Queensland, Brisbane, 306 Carmody Road, St Lucia, QLD, 4072, Australia

[○]Lehrstuhl für Biochemie, Universität Bayreuth, Universitätsstraße 30, 95447 Bayreuth, Germany

[◆]School of Chemistry and Biomedical and Health Research Centre, University of Leeds, Leeds, LS2 9JT, United Kingdom

[¶]Laboratoire de Chimie de Coordination du CNRS, 205 route de Narbonne, 31077 Toulouse, France

Author Contributions

[⊥]These authors contributed equally.

Notes

The authors declare no competing financial interest.

■ ACKNOWLEDGMENTS

This work was supported by the Deutsche Forschungsgemeinschaft, the Max-Planck-Gesellschaft, and the Zentrum für Angewandte Chemische Genomik. C.D. and R.S.B. thank the Alexander von Humboldt-Stiftung for fellowships. We thank the X-ray communities of the Max Planck Institute of Molecular Physiology (Dortmund, Germany) and the Max Planck Institute of Medical Research (Heidelberg, Germany) for collecting diffraction data at the Swiss Light Source of the Paul Scherrer Institute (Villigen, Switzerland) and for giving us generous access to and support for station X10SA.

■ REFERENCES

(1) Konstantinopoulos, P. A.; Karamouzis, M. V.; Papavassiliou, A. G. *Nat. Rev. Drug Discovery* **2007**, *6*, 541−555.

(2) Stenmark, H. *Nat. Rev. Mol. Cell Biol.* **2009**, *10*, 513−525.

(3) Coxon, F. P.; Helfrich, M. H.; Larijani, B.; Muzylak, M.; Dunford, J. E.; Marshall, D.; McKinnon, A. D.; Nesbitt, S. A.; Horton, M. A.; Seabra, M. C.; Ebetino, F. H.; Rogers, M. J. *J. Biol. Chem.* **2001**, *276*, 48213−48222.

(4) Roelofs, A. J.; Hulley, P. A.; Meijer, A.; Ebetino, F. H.; Russell, R. G.; Shipman, C. M. *Int. J. Cancer* **2006**, *119*, 1254−1261.

(5) Lackner, M. R.; Kindt, R. M.; Carroll, P. M.; Brown, K.; Cancilla, M. R.; Chen, C.; de, S. H.; Franke, Y.; Guan, B.; Heuer, T.; Hung, T.; Keegan, K.; Lee, J. M.; Manne, V.; O'Brien, C.; Parry, D.; Perez-Villar, J. J.; Reddy, R. K.; Xiao, H.; Zhan, H.; Cockett, M.; Plowman, G.; Fitzgerald, K.; Costa, M.; Ross-Macdonald, P. *Cancer Cell* **2005**, *7*, 325−336.

(6) Mitra, S.; Cheng, K. W.; Mills, G. B. *Semin. Cell Dev. Biol.* **2011**, *22*, 57−68.

(7) Cheng, K. W.; Lahad, J. P.; Kuo, W. L.; Lapuk, A.; Yamada, K.; Auersperg, N.; Liu, J.; Smith-McCune, K.; Lu, K. H.; Fishman, D.; Gray, J. W.; Mills, G. B. *Nat. Med.* **2004**, *10*, 1251−1256.

(8) Bon, R. S.; Guo, Z.; Stigter, E. A.; Wetzel, S.; Menninger, S.; Wolf, A.; Choidas, A.; Alexandrov, K.; Blankenfeldt, W.; Goody, R. S.; Waldmann, H. *Angew. Chem., Int. Ed.* **2011**, *50*, 4957−4961.

(9) Guo, Z.; Wu, Y. W.; Tan, K. T.; Bon, R. S.; Guiu-Rozas, E.; Delon, C.; Nguyen, T. U.; Wetzel, S.; Arndt, S.; Goody, R. S.; Blankenfeldt, W.; Alexandrov, K.; Waldmann, H. *Angew. Chem., Int. Ed.* **2008**, *47*, 3747−3750.

(10) McKenna, C. E.; Kashemirov, B. A.; Blazewska, K. M.; Mallard-Favier, I.; Stewart, C. A.; Rojas, J.; Lundy, M. W.; Ebetino, F. H.; Baron, R. A.; Dunford, J. E.; Kirsten, M. L.; Seabra, M. C.; Bala, J. L.; Marma, M. S.; Rogers, M. J.; Coxon, F. P. *J. Med. Chem.* **2010**, *53*, 3454−3464.

(11) Tan, K. T.; Guiu-Rozas, E.; Bon, R. S.; Guo, Z.; Delon, C.; Wetzel, S.; Arndt, S.; Alexandrov, K.; Waldmann, H.; Goody, R. S.; Wu, Y. W.; Blankenfeldt, W. *J. Med. Chem.* **2009**, *52*, 8025−8037.

(12) Watanabe, M.; Fiji, H. D.; Guo, L.; Chan, L.; Kinderman, S. S.; Slamon, D. J.; Kwon, O.; Tamanoi, F. *J. Biol. Chem.* **2008**, *283*, 9571−9579.

(13) Wu, Y. W.; Waldmann, H.; Reents, R.; Ebetino, F. H.; Goody, R. S.; Alexandrova, K. *ChemBioChem* **2006**, *7*, 1859−1861.

(14) Wu, Y. W.; Alexandrov, K.; Brunsveld, L. *Nat. Protoc.* **2007**, *2*, 2704−2711.

(15) Neamati, N.; Hong, H.; Mazumder, A.; Wang, S.; Sunder, S.; Nicklaus, M. C.; Milne, G. W.; Proksa, B.; Pommier, Y. *J. Med. Chem.* **1997**, *40*, 942−951.

(16) Hidalgo, M. E.; Fernandez, E.; Quilhot, W.; Lissi, E. *Phytochemistry* **1994**, *37*, 1585−1587.

(17) Muller, K. *Appl. Microbiol. Biotechnol.* **2001**, *56*, 9−16.

(18) Correche, E. R.; Enriz, R. D.; Piovano, M.; Garbarino, J.; Gomez-Lechon, M. J. *Altern. Lab Anim.* **2004**, *32*, 605−615.

(19) Sala, T.; Sargent, M. V. *J. Chem. Soc., Perkin Trans. 1* **1979**, 2593−2598.

(20) Kulkarni, N. N.; Kulkarni, V. S.; Lele, S. R.; Hosangadi, B. D. *Tetrahedron* **1988**, *44*, 5145−5149.

(21) Guo, Z.; Wu, Y. W.; Das, D.; Delon, C.; Cramer, J.; Yu, S.; Thuns, S.; Lupilova, N.; Waldmann, H.; Brunsveld, L.; Goody, R. S.; Alexandrov, K.; Blankenfeldt, W. *EMBO J.* **2008**, *27*, 2444−2456.

(22) Zhang, H.; Seabra, M. C.; Deisenhofer, J. *Structure* **2000**, *8*, 241−251.

(23) Lane, K. T.; Beese, L. S. *J. Lipid Res.* **2006**, *47*, 681−699.